



# Depletion-Induced Chiral Chain Formation of Magnetic Spheres

Sandrine M.F. Heijnen, Patrick van Vliet, Bonny W.M. Kuipers, Albert P. Philipse, Andrei V. Petukhov\*  and Samia Ouhajji <sup>†,\*</sup> 

Van 't Hoff Laboratory for Physical and Colloid Chemistry, Debye Institute for Nanomaterials Science, Utrecht University, Padualaan 8, 3584 CH Utrecht, the Netherlands

\* Correspondence: Ouhajji@Physics.LeidenUniv.nl (S.O); A.V.Petukhov@uu.nl (A.V.P.)

† Current address: Soft Matter Physics, Huygens-Kamerlingh Onnes Lab, Niels Bohrweg 2, 2333 CA Leiden, Leiden University, the Netherlands

**Abstract:** Experimental evidence is presented for the spontaneous formation of chiral configurations in bulk dispersions of magnetized colloids that interact by a combination of anisotropic dipolar interactions and isotropic depletion attractions. The colloids are superparamagnetic silica spheres, magnetized and aligned by a carefully tuned uniform external magnetic field; isotropic attractions are induced by using poly(ethylene oxide) polymers as depleting agents. At specific polymer concentrations, sphere chains wind around each other to form helical structures – of the type that previously have only been observed in simulations on small sets of unconfined dipolar spheres with additional isotropic interactions.

**Keywords:** chirality; depletion-interaction; superparamagnetic colloids

## 1. Introduction

Chirality is a property of geometrical objects, the mirror image of which is not superimposable with the original [1]. Kelvin coined the term ‘chirality’, from the Greek  $\chi\epsilon\iota\rho$  for *hand* – perhaps the most familiar example of a chiral object [2,3]. While physical properties, such as melting temperature or colour, of left- and right-handed molecules are identical, the handedness of a molecule sensitively affects its odour, toxicity and optical activity for instance [1,2]. Chiral isomers of the molecule limonene, for example, are responsible for the distinct aroma of lemons versus that of oranges [4].

The absence of inversion symmetry manifests itself over many length scales; from the double helix of DNA to the coiling of cucumber tendrils [5] and chiral liquid crystals [6–8]. Whereas achiral rods can form a nematic phase with long-range orientational order but no positional ordering, chiral rods can transform the nematic into a chiral nematic (also known as cholesteric) phase in which the orientation of the rods rotates over a macroscopic distance.

Two systems exhibiting spontaneous chiral symmetry breaking were studied theoretically by Pickett et al. [9] One system employs close-packed isotropic spheres that form helical structures upon cylindrical confinement due to geometrical restrictions [10,11]. Macroscopically this can be demonstrated by filling a measuring cylinder with marbles of the proper size ratio. Experimentally this was realized by the formation of helical chains from colloidal spheres confined in V-grooves by capillary forces [12]. Jiang et al. demonstrated this helical chain formation via the co-assembly of colloids and microtubes [13] and Ouhajji et al. developed a method to fix the assembled chiral colloids together [14,15].

The second system comprises unconfined dipolar hard spheres with an additional isotropic attraction that were found to exhibit chiral ground states in simulations [9]. These simulations were performed for chains containing 15 aligned spheres with embedded dipole moments which, for certain values of the strength and range of the attraction,

**Citation:** Heijnen, S.M.F.; Van Vliet, P.; Kuipers, B.W.M.; Philipse, A.P.; Petukhov, A.V.; Ouhajji, S. Depletion-Induced Chiral Chain Formation of Magnetic Spheres. *Materials* **2021**, *1*, 0.

<https://dx.doi.org/>

Received:

Accepted:

Published:

**Publisher’s Note:** MDPI stays neutral with regard to jurisdictional claims in published maps and institutional affiliations.

**Copyright:** © 2021 by the authors. Submitted to *Materials* for possible open access publication under the terms and conditions of the Creative Commons Attribution (CC BY) license (<https://creativecommons.org/licenses/by/4.0/>).

37 formed helical structures. The observed chiral structures mainly consisted of three chains  
38 winding around each other.

39 Here, we demonstrate experimentally the arrangement of unconfined dipolar par-  
40 ticles into helical chains due to isotropic attraction caused by depleting polymers. To  
41 this end, we employ negatively charged superparamagnetic silica spheres as dipolar  
42 spheres. Salt is added to reduce the Debye length and to effectively obtain dipolar hard  
43 spheres. Addition of the polymer poly(ethylene oxide) generates an additional attraction  
44 between the particles in the form of depletion interaction. An external homogeneous  
45 magnetic field is applied to align the magnetic particles in a sea of depletants with  
46 varying concentrations.

## 47 **2. Materials and Methods**

### 48 *2.1. Materials*

49 Superparamagnetic silica colloids in water with a diameter (specified by the man-  
50 ufacturer) of  $0.51 \mu\text{m} \pm 0.03 \mu\text{m}$  and iron oxide content  $\geq 30\%$  were purchased from  
51 microParticles GmbH. Poly(ethylene oxide) (PEO, 600 kDa) was purchased from Sigma-  
52 Aldrich, sodium chloride (p.a.) from Merck and sodium azide ( $\geq 99\%$ ) from Fisher  
53 Scientific. All chemicals were used as received. All water used was purified by a Milli-Q  
54 water purification system.

### 55 *2.2. Magnetic Field*

56 A Helmholtz cube was developed for *in situ* observation of colloids in a homo-  
57 geneous magnetic field, see Supporting Information and Figure S1. Three pairs of  
58 Helmholtz coils were arranged orthogonally producing a three-dimensional magnetic  
59 field.

### 60 *2.3. Optical Microscopy*

61 Optical microscopy images were obtained using a Nikon Eclipse Ti-E inverted  
62 microscope equipped with a *the Imaging Source* DMK 23UX174 Digital Camera. A  
63 Nikon CFI Apo TIRF objective ( $100\times$  magnification, N.A. 1.49) was used. Pictures were  
64 recorded in bright field mode. Samples were prepared by mixing desired amounts of  
65 stock solutions of superparamagnetic silica spheres, PEO and salt in vials and hollow  
66 glass tubes ( $0.1\times 2\times 50$  mm, VitroCom) were filled with these mixtures by capillary  
67 action. The tubes were sealed with optical adhesive (Norland 81) that was cured with  
68 UV-light (wavelength of 365 nm, 6 W UVP UVGL-58 lamp) and sealed with a layer of  
69 nail polish to prevent solvent evaporation. Samples consisted of varying concentrations  
70 superparamagnetic colloids and PEO, and 10 mM sodium chloride. Sodium chloride  
71 was occasionally (partially) replaced by sodium azide (while keeping the total ionic  
72 strength constant) to suppress bacterial growth.

## 73 **3. Results and Discussion**

### 74 *3.1. Model System*

75 We used negatively charged superparamagnetic silica spheres as dipolar spheres  
76 to determine experimentally if unconfined dipolar particles with an isotropic attraction  
77 arrange into helical chains. Two batches of commercial superparamagnetic silica spheres  
78 were used with diameters ( $2R_c$ ) of  $566 \pm 18$  nm and  $548 \pm 14$  nm, as determined with  
79 TEM (see Figure S4a in Supporting information). In the absence of an external magnetic  
80 field, well-dispersed spheres can be observed in water, see Figure S4b. 10 mM salt was  
81 added to reduce the Debye screening length to 3 nm (see Appendix A). At this ionic  
82 strength, colloidal stability was maintained while the double-layer interactions were  
83 considerably screened, resulting in effectively dipolar hard spheres.

84 In the numerical simulations by Pickett et al. [9], the applied pairwise attractive  
85 potential was modelled by:

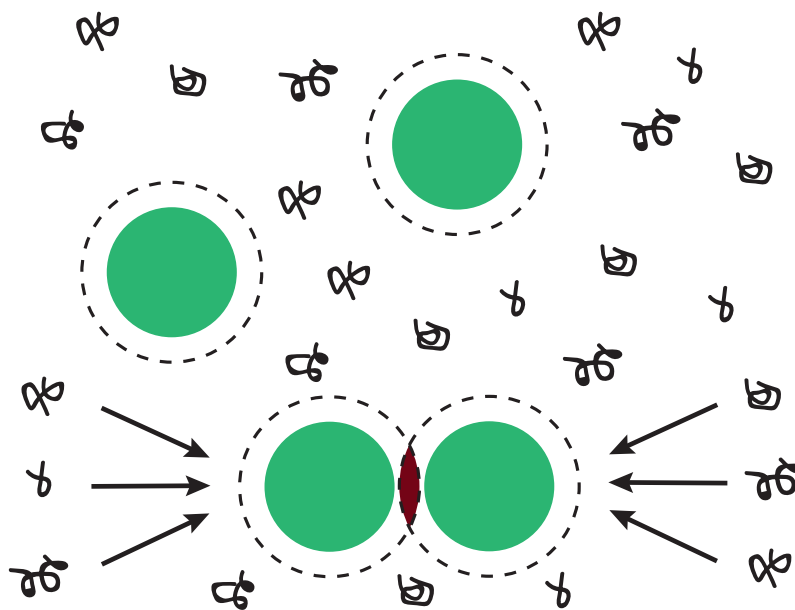


**Figure 1.** Schematic depiction of depletion interaction. In a mixture of colloidal spheres and non-adsorbing polymer, a depletion layer arises around the spheres as indicated by the dashed circles [16]. The centre of mass of the polymer is excluded (depleted) from this layer due to loss of configurational entropy. When two or more depletion layers overlap, the free volume available for the polymers increases. The polymers thus exert a net osmotic pressure on the colloids forcing the particles together.

$$U_{\text{attr}}(r) = \begin{cases} -\epsilon \frac{R-r}{R-2R_c} & 2R_c \leq r \leq R \\ 0 & \text{otherwise} \end{cases}, \quad (1)$$

86 as a function of the distance  $r$  between two spheres. Here,  $\epsilon$  defines the strength and  $R$   
 87 the range of the attraction. Experimentally, isotropic attraction between particles can  
 88 be achieved through the addition of non-adsorbing polymers. In a mixture of colloids  
 89 and non-adsorbing polymer, negative adsorption of a polymer chain results in a loss of  
 90 configurational entropy due to a depletion layer around the colloid which the centre  
 91 of mass of the polymer cannot penetrate, see Figure 1 [16]. To minimize their free  
 92 energy, the polymers exert a net osmotic pressure on the colloids forcing the particles  
 93 together. This apparent attraction between the colloidal particles is named the depletion  
 94 interaction. It is an apparent attraction as depletion is entropically driven and arises as a  
 95 result of purely repulsive colloid-colloid and colloid-polymer interactions. The range of  
 96 the depletion potential is determined by the size of the depletant, whereas the attraction  
 97 strength depends on the osmotic pressure and thus on the depletant concentration.  
 98 Therefore, the strength and the range of the attraction between colloids can be modified  
 99 independently using depletion forces.

100 In Figure 2 it is shown that in the limit of small  $q$ , the Asakura-Oosawa-Vrij (AOV)  
 101 depletion potential [16,17] approximates the potential given in Equation 1 reasonably  
 102 well. To compare the two potentials, the following conversion was applied:  $R = q + 1$ .  
 103 As depletant, PEO was used with a molecular weight of 600 kDa and a (calculated) radius  
 104 of gyration  $R_g$  of 50 nm (see Appendix A) [18]. The size ratio  $q$  of the polymer-colloid  
 105 mixture is thus equal to  $R_g/R_c = 0.18$ .

106 An external magnetic field is applied to align the magnetic particles in a sea of  
 107 depletants with varying concentrations. A Helmholtz cube was developed for *in situ*  
 108 observation of colloids in a homogeneous magnetic field, see Supporting Information  
 109 and Figure S1, as an inhomogeneous magnetic field resulted in (reversible) lateral  
 110 aggregation (See Supporting Information and Figures S2 and S3).

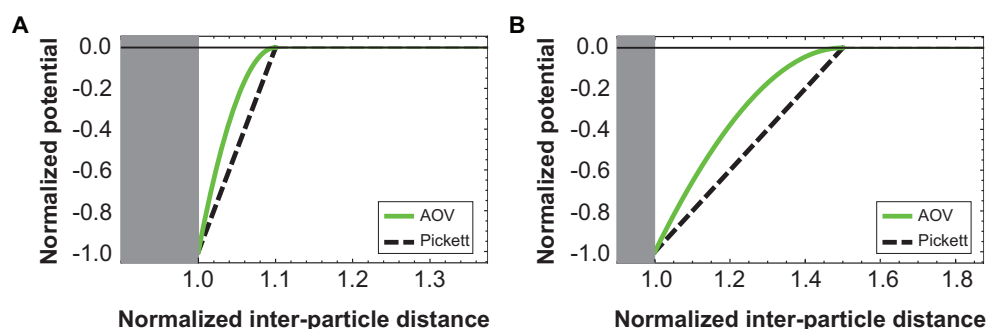


**Figure 2.** Comparison of potentials. AOV depletion potential and the potential as given in Equation 1 (denoted here as Pickett potential) normalized to the contact potential as a function of normalized inter-particle distance for (a)  $q = 0.1$  and (b)  $q = 0.5$ . For small  $q$ , the two potentials are fairly similar.

### 111 3.2. Observations

112 Samples containing 50 mg/mL superparamagnetic silica particles, 10 mM salt and  
 113 PEO concentrations ranging from 0 mg/mL to 1 mg/mL were placed in the homoge-  
 114 neous magnetic field of the Helmholtz cube. This polymer concentration corresponds to  
 115 depletion potentials of 0.5 to 6  $k_B T$  (see Appendix A). A magnetic field of 3 mT results  
 116 in an interaction strength on the order of  $-65 k_B T$  (assuming point dipole-dipole inter-  
 117 actions), which is sufficient to induce chain formation of the superparamagnetic silica  
 118 spheres. However, in a homogeneous magnetic field of 3 mT, mixtures of magnetic silica  
 119 spheres, salt and depletant do not form chiral structures, see Figure 3. By lowering the  
 120 magnetic field strength to 1.4 mT (dipolar hard sphere interaction at contact of  $-4 k_B T$ ),  
 121 two adjacent linear sphere chains wind around each other at three depletant concentra-  
 122 tions, see Figure 4 and Supporting Videos. Typically, images and videos were recorded  
 123 after one hour of equilibration. Chains start to form immediately upon switching the  
 124 magnetic field on. After approximately one hour, nearly all particles in dispersion are  
 125 found in chains (see Supporting Video). Upon removing the magnetic field, structures  
 126 fall apart immediately in this completely reversible process (see Supporting Video).  
 127 Both left- and right-handed structures occur with equal probability as expected for a  
 128 spontaneous symmetry breaking process. Most structures showed one twist with the  
 129 pitch increasing with the length of the chains and thus the number of spheres per chain.

130 These long chains of entwined spherical particles did not form in the absence of  
 131 depletant or at higher magnetic field strengths. In a magnetic field of 3 mT, the dipole-  
 132 dipole interactions are much stronger compared to the depletion potential and rigid  
 133 linear chains dominate. More dynamic structures can be obtained in a weaker magnetic  
 134 field, due to competing dipolar and depletion interactions, allowing the exploration of  
 135 more configurations and ultimately the formation of helical sphere chains. In a helical  
 136 arrangement, the particles accommodate more neighbours leading to an increase in  
 137 the entropy of the depleting agent while winding allows the system to minimize the  
 138 magnetic interaction energy.

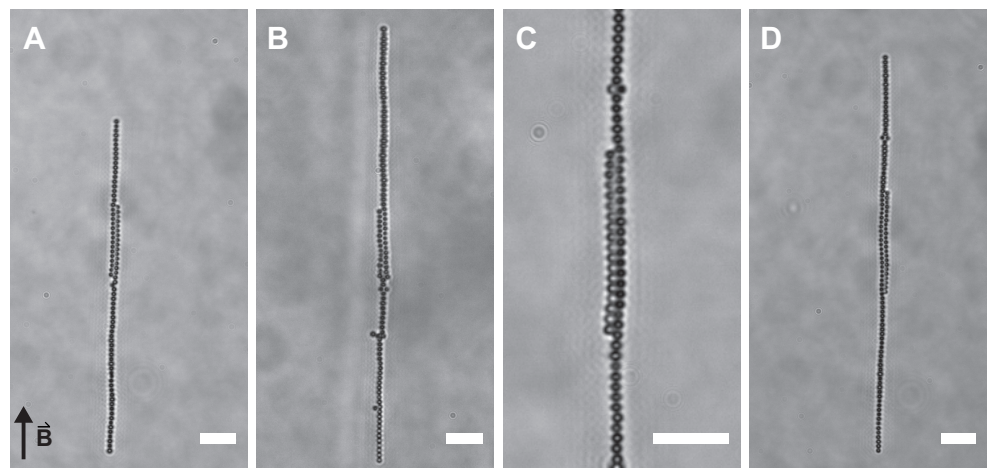


**Figure 3.** Linear sphere chains. In a homogeneous magnetic field of 3 mT, linear sphere chains are formed for all studied concentrations of PEO. (a) 0 mg/mL, (b) 0.10 mg/mL, (c) 0.14 mg/mL and (d) 0.16 mg/mL PEO. Scale bars are 5  $\mu\text{m}$ . All images were taken approximately one hour after switching the magnetic field on. The arrow indicates the direction of the applied field in all images.

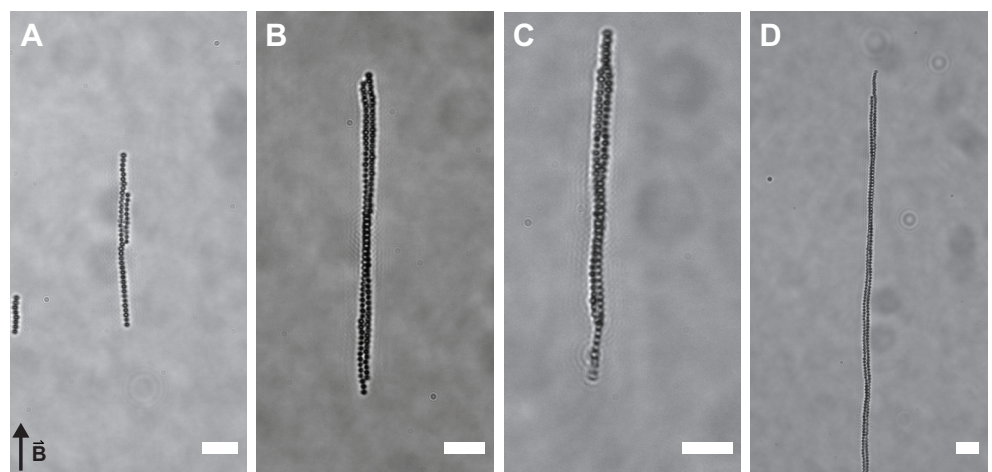


**Figure 4.** Helical sphere chains. In a homogeneous magnetic field of 1.4 mT, long chains of spheres wind around each other forming helical chains in the presence of depletant. (a) 0 mg/mL, (b) 0.10 mg/mL, (c) 0.14 mg/mL and (d) 0.16 mg/mL PEO. Scale bars are 5  $\mu\text{m}$ . All images were taken approximately one hour after switching the magnetic field on. The arrow indicates the direction of the applied field in all images.

### 139 3.3. Comparison with Simulations

140 Upon introduction of an additional isotropic attraction, unconfined dipolar spheres  
 141 arrange into helical bundles, both *in silico* and *in vitro*. However, whereas in the simulations  
 142 three chains of spheres were found to wind around each other, in the experiments  
 143 no more than two chains of spheres arranged to form a twisted structure. Even at higher  
 144 magnetic field strengths, not more than two parallel chains were observed. Thereby,  
 145 the simulations were limited to 15 particles in total; a substantially larger amount of  
 146 particles were employed experimentally leading to vastly larger helical structures.

147 In Figure 5, our experimental results are presented in a phase diagram together with  
 148 the simulation results of Pickett et al. [9]. Only a small part of the available phase space  
 149 could be probed by the chosen experimental model system as it is limited to small  $q$ .  
 150 Employing larger PEO polymers would result in a deviation from the required pairwise  
 151 potential as discussed previously. Likewise, smaller dipolar spheres would impede  
 152 characterization with optical microscopy. The experimental helical structures are found



153 close to the theoretically predicted conditions with one point overlapping in the phase  
 154 diagram. This indicates that a correct model system was chosen. Small deviations can  
 155 be explained by the discrepancy in the applied potentials.

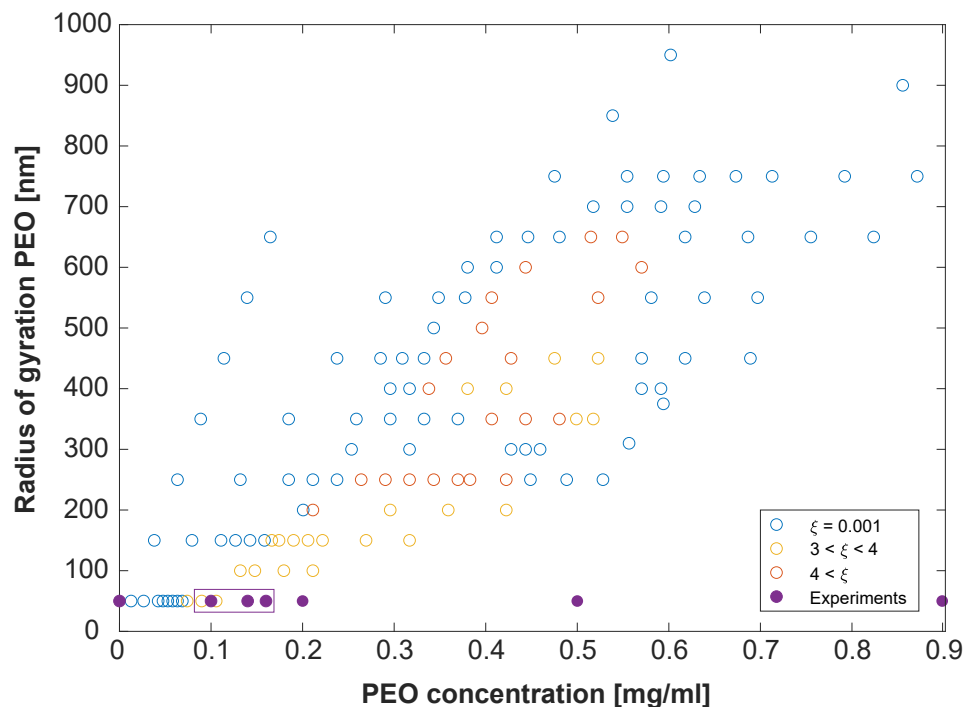


**Figure 5.** Phase diagram. Spontaneous symmetry breaking as a function of the radius of gyration and the concentration of PEO. Open circles indicate the theoretical results obtained by Pickett et al. [9]. These are colour-coded with the chiral order parameter, *i.e.* the amount of chirality of a structure. The blue open circles are achiral states whereas the yellow and orange open circles indicate two different chiral states. The filled circles are the experimental data points as discussed in this Article. The points enclosed inside the box are chiral, whereas those outside of the box are achiral. One point overlaps. Experimental data points were obtained in a homogeneous magnetic field of 1.4 mT with silica particle concentration of 50 mg/mL and 10 mM salt.

#### 156 4. Conclusions

157 We have shown experimentally the spontaneous formation of chiral chains from  
 158 dispersions of magnetic colloids and depleting polymers in an external magnetic field.  
 159 For specific depletant concentrations, chains of spheres are found to wind around each  
 160 other forming helical structures. These structures maximize overlap of exclusion zones  
 161 between neighbouring spheres and, hence, lower the free energy of the system. Our  
 162 findings confirm for the first time the theoretical prediction that unconfined dipolar  
 163 spheres with an additional isotropic attraction form helical structures. A topic for  
 164 future investigations is the functionalization of the superparamagnetic silica spheres  
 165 with photo-responsive molecules to obtain permanent sphere chains. Upscaling of the  
 166 permanently fixed chiral chains could then lead to the study of colloidal chiral liquid  
 167 crystals.

168 **Supplementary Materials:** The following are available online at <https://www.mdpi.com/1996-1944/1/1/0/s1>, Figure S1: Helmholtz cube, Figure S2: linear sphere chains, Figure S3: helical sphere chains, Figure S4: superparamagnetic silica spheres, Table S1: properties of the three pairs of Helmholtz coils, Video S1: formation of linear chains in a magnetic field of 3 mT (video is sped up, total duration: 1 hour), Video S2: chiral chain of magnetic spheres in magnetic field of 1.4 mT, Video S3: long chiral chain of magnetic spheres in magnetic field of 1.4 mT, Video S4: chiral chain falling apart upon turning off the magnetic field.

175 **Author Contributions:** Conceptualization, A.P.P., A.V.P. and S.O.; methodology, A.P.P., A.V.P.  
 176 and S.O.; validation, S.M.F.H. and S.O.; formal analysis, S.M.F.H., P.V.V. and S.O.; investigation,  
 177 S.M.F.H., P.V.V., B.W.M.K. and S.O.; resources, B.W.M.K.; data curation, S.O.; writing—original  
 178 draft preparation, S.O.; writing—review and editing, A.P.P., A.V.P. and S.O.; visualization, S.M.F.H.,  
 179 P.V.V. and S.O.; supervision, A.P.P., A.V.P. and S.O.; project administration, A.P.P., A.V.P. and S.O.;  
 180 funding acquisition, A.P.P. and A.V.P. All authors have read and agreed to the published version  
 181 of the manuscript.

182 **Funding:** This research was funded by The Netherlands Organisation for Scientific Research  
 183 (NWO) grant number 712.014.002.

184 **Institutional Review Board Statement:** Not applicable.

185 **Informed Consent Statement:** Not applicable.

186 **Acknowledgments:** Álvaro González García is thanked for useful discussions. We thank Mar-  
 187 cel van Asselen of the Engineering group of the Scientific Instrumentation department for the  
 188 mechanical design and Manfred van den Berg, Helge Veltman and co-workers of the Production  
 189 group of the Faculty of Science at Utrecht University for the realization of the Helmholtz setup.

190 **Conflicts of Interest:** The authors declare no conflict of interest.

## 191 Appendix A. Calculations

### 192 Appendix A.1. Debye Screening Length

193 The electric potential profile surrounding a colloidal particle approaches zero at a  
 194 distance of several times the Debye screening length  $\kappa^{-1}$  given by:

$$\kappa^{-1} = \sqrt{\frac{\epsilon_0 \epsilon_r k_B T}{2e^2 n_0}}. \quad (\text{A1})$$

195 Here,  $\epsilon_0$  is the vacuum permittivity,  $\epsilon_r$  is the dielectric constant of the medium,  $k_B$  is the  
 196 Boltzmann constant,  $T$  is the absolute temperature,  $e$  is the elementary charge and  $n_0$   
 197 the particle density at the point where the field is zero. In water at 25 °C, Equation A1  
 198 reduces to:

$$\kappa^{-1} = \frac{0.30}{\sqrt{c}} \text{ nm}, \quad (\text{A2})$$

199 with  $c$  the salt concentration in mol/L.[19]

### 200 Appendix A.2. Radius of Gyration

201 Devanand and Selser studied the behaviour of PEO in water with static and dy-  
 202 namic light scattering measurements.[18] In a good solvent, the following relation holds  
 203 between the radius of gyration  $R_g$  and molecular weight  $M_w$  (in g/mol):

$$R_g = 0.215 M_w^{0.583 \pm 0.031} \text{ \AA} \quad (\text{A3})$$

### 204 Appendix A.3. Depletion Potential

205 The depletion potential between two spheres  $W(h)$  due to ideal polymers is, in the  
 206 Derjaguin approximation, given by:[16]

$$W(h) = -n_b k_B T R_c R_g^2 \left( 4\pi \ln 2 - 4\sqrt{\pi} \frac{h}{R_g} + \frac{\pi h^2}{2 R_g^2} \right). \quad (\text{A4})$$

207 Here,  $n_b$  is the bulk number density of ideal polymers,  $R_c$  is the radius of the spheres,  
 208  $R_g$  is the radius of gyration of the polymer and  $h$  is the separation between two spheres.  
 209 The strength of the interaction or the depth of the potential  $\epsilon$  at contact ( $h = 0$ ) is thus:

$$\epsilon = \frac{W(h)}{k_B T} = -n_b R_c R_g^2 4\pi \ln 2 \quad (\text{A5})$$

## References

1. Ma, W.; Xu, L.; de Moura, A.F.; Wu, X.; Kuang, H.; Xu, C.; Kotov, N.A. Chiral Inorganic Nanostructures. *Chem. Rev.* **2017**, *117*, 8041–8093. doi:10.1021/acs.chemrev.6b00755.
2. Harris, A.B.; Kamien, R.D.; Lubensky, T.C. Molecular chirality and chiral parameters. *Rev. Mod. Phys.* **1999**, *71*, 1745–1757. doi:10.1103/RevModPhys.71.1745.
3. Zafar, M.; Ragusa, A. Chirality at the Nanoparticle Surface: Functionalization and Applications. *Appl. Sci.* **2020**, *10*, 5357.
4. Nayani, K.; Kim, Y.K.; Abbott, N.L. Chiral interactions in liquid crystals. *Nat. Mater.* **2018**, *17*, 14–15.
5. Gerbode, S.J.; Puzey, J.R.; McCormick, A.G.; Mahadevan, L. How the Cucumber Tendril Coils and Overwinds. *Science* **2012**, *337*, 1087–1091. doi:10.1126/science.1223304.
6. Barry, E.; Hensel, Z.; Dogic, Z.; Shribak, M.; Oldenbourg, R. Entropy-Driven Formation of a Chiral Liquid-Crystalline Phase of Helical Filaments. *Phys. Rev. Lett.* **2006**, *96*, 018305. doi:10.1103/PhysRevLett.96.018305.
7. Wensink, H.H.; Morales-Anda, L. Chiral assembly of weakly curled hard rods: Effect of steric chirality and polarity. *J. Chem. Phys.* **2015**, *143*, 144907. doi:10.1063/1.4932979.
8. Collings, P.; Hird, M. *Introduction to Liquid Crystals: Chemistry and Physics*; Taylor & Francis, 1997.
9. Pickett, G.T.; Gross, M.; Okuyama, H. Spontaneous Chirality in Simple Systems. *Phys. Rev. Lett.* **2000**, *85*, 3652–3655.
10. Mughal, A.; Chan, H.K.; Weaire, D. Phyllotactic Description of Hard Sphere Packing in Cylindrical Channels. *Phys. Rev. Lett.* **2011**, *106*, 115704. doi:10.1103/PhysRevLett.106.115704.
11. Mughal, A.; Chan, H.K.; Weaire, D.; Hutzler, S. Dense packings of spheres in cylinders: Simulations. *Phys. Rev. E* **2012**, *85*, 051305. doi:10.1103/PhysRevE.85.051305.
12. Yin, Y.; Xia, Y. Self-assembly of spherical colloids into helical chains with well-controlled handedness. *J. Am. Chem. Soc.* **2003**, *125*, 2048–2049.
13. Jiang, L.; de Folter, J.W.J.; Huang, J.; Philipse, A.P.; Kegel, W.K.; Petukhov, A.V. Helical colloidal sphere structures through thermo-reversible co-assembly with molecular microtubes. *Angew. Chem., Int. Ed.* **2013**, *52*, 3364–3368.
14. Ouhajji, S.; van Ravensteijn, B.G.P.; Fernández-Rico, C.; Lacina, K.S.; Philipse, A.P.; Petukhov, A.V. Wet-Chemical Synthesis of Chiral Colloids. *ACS Nano* **2018**, *12*, 12089–12095. doi:10.1021/acsnano.8b05065.
15. Ouhajji, S. *Chiral and Active Colloids*; PhD Thesis, 2019.
16. Lekkerkerker, H.N.W.; Tuinier, R. *Colloids and the Depletion Interaction*; Springer Netherlands, 2011.
17. Asakura, S.; Oosawa, F. On Interaction between Two Bodies Immersed in a Solution of Macromolecules. *J. Chem. Phys.* **1954**, *22*, 1255–1256.
18. Devanand, K.; Selser, J.C. Asymptotic behavior and long-range interactions in aqueous solutions of poly(ethylene oxide). *Macromolecules* **1991**, *24*, 5943–5947. doi:10.1021/ma00022a008.
19. Israelachvili, J.N. *Intermolecular and Surface Forces (Third Edition)*; Academic Press, 2011.